OPEN

NPG Asia Materials (2016) 8, e277; doi:10.1038/am.2016.70
www.nature.com/am

ORIGINAL ARTICLE

Handheld energy-efficient magneto-optical real-time quantitative PCR device for target DNA enrichment and quantification

Tsung-Ju Li[1,9], Chen-Min Chang[2,9], Po-Yang Chang[3], Yu-Chun Chuang[4], Chih-Chia Huang[3,5], Wu-Chou Su[1,6,7] and Dar-Bin Shieh[1,2,5,7,8]

A PCR provides not only valuable genetic information that enables precise differential disease diagnosis but also quantitative data to assess various clinical states. We report the successful integration of novel dual-mode magnetic Fe_3O_4 nanoclusters that deliver photothermal conversion. The clusters can be excited with pulsed laser light for precision thermal cycle modulation to develop an ultrafast quantitative PCR system. Traditional PCR heats and cools the sample from outside the PCR tube; the heat needs to pass through the heat block, tube wall and transfer to the DNA through water molecules. In contrast, our system uses nanoparticles inside the liquid phase as numerous 'nanoheaters'; thus the thermal transfer between particles and adjacent water or DNA molecules becomes extremely efficient because of proximity at the molecular level. Moreover, the defective mitochondrial DNA from cybrid cell lines of a patient with chronic progressive external ophthalmoplegia syndrome, a mitochondrial disease, was efficaciously detected. The system has a simple design, is extremely energy efficient and is faster than traditional qPCR. Our finding provides new insight into rapid and accurate quantitative diagnostics for future point-of-care applications.
NPG Asia Materials (2016) **8,** e277; doi:10.1038/am.2016.70; published online 3 June 2016

INTRODUCTION

Rapid and accurate quantitative gene diagnostics is a highly desirable emerging trend for point-of-care devices. Since the invention of the PCR in 1985,[1] and the later implementation of quantitative PCR (qPCR) technologies, using such sensitive and specific DNA amplification and quantitative methods have become the norm in a wide variety of biomedical applications. Their use in advanced medical diagnostics has become essential in daily clinical practice and has significantly augmented health-care quality and disease control. However, current PCR systems are still quite limited for advanced point-of-care applications because of their large size, weight, slow signal amplification speed and high energy consumption. One of the major hurdles is the heating and cooling mechanism, which requires a large heat sink and high driving power.[2,3] New technologies based on microfluidic systems, such as chip-PCR or real-time capillary convective PCR, have greatly shortened detection time and require far fewer DNA samples because of the improved heat-transfer efficiency in the designed microscale compartment space.[4] However, these systems still require an external pump to drive the fluid dynamics and micro heaters,[5,6] thus significantly increasing the complexity, energy consumption and overall size of the systems, which makes them less portable and less efficient.

The surface plasmon resonance property of gold (Au) nanorods is well known for efficient photothermal conversion with excitation wavelengths associated with their aspect ratio.[7] Many studies[8,9] have reported that Au nanorods and nanoparticles are excellent plasmonic photothermal heating sources for hyperthermal therapy. Photothermal conversion has been postulated for micro heating sources in other genetic applications.[10,11] However, the unstable thermodynamic properties of Au nanorods at high temperature make them unsuitable components for continuous heat-transfer agents, which makes Au-nanoparticle-based PCR a great challenge.[12] Recently, Lee *et al.*[13] fabricated thin Au film as a heat interface for a PCR reaction. This design showed excellent temperature accuracy and stability using photon excitation at 450 nm. However, when used with real-time PCR, this wavelength might present a lot of challenges because many

[1]Institute of Basic Medical Sciences, College of Medicine, National Cheng Kung University, Tainan, Taiwan; [2]Institute of Oral Medicine, College of Medicine, National Cheng Kung University, Tainan, Taiwan; [3]Department of Photonics, National Cheng Kung University, Tainan, Taiwan; [4]National Synchrotron Radiation Research Center, Hsinchu, Taiwan; [5]Advanced Optoelectronic Technology Center and Center for Micro/Nano Science and Technology, National Cheng Kung University, Tainan, Taiwan; [6]Cancer center and Department of Internal Medicine, National Cheng Kung University Hospital, Tainan, Taiwan; [7]Institute of Clinical Medicine, National Cheng Kung University College of Medicine and Hospital, Tainan, Taiwan and [8]Department of Stomatology, National Cheng Kung University Hospital, Tainan, Taiwan
[9]These authors contributed equally to this work and should be considered co-first authors.
Correspondence: Professor C-C Huang, Department of Photonics, National Cheng Kung University, Tainan 701, Taiwan.
E-mail: c2huang@mail.ncku.edu.tw
or Professor W-C Su, Cancer center and Department of Internal Medicine, National Cheng Kung University Hospital, Tainan 704, Taiwan.
E-mail: sunnysu@mail.ncku.edu.tw
or Professor D-B Shieh, Institute of Oral Medicine and Department of Stomatology, National Cheng Kung University, Tainan 701, Taiwan.
E-mail: dbshieh@mail.ncku.edu.tw
Received 22 December 2015; revised 26 March 2016; accepted 31 March 2016

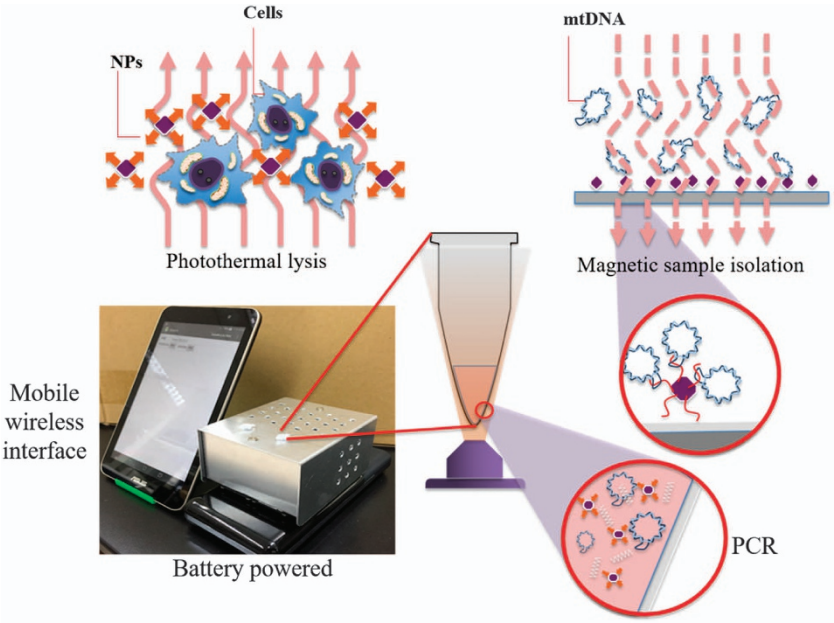

Figure 1 A schematic diagram for real-time PCR integrated with a highly efficient magnetic field driven molecular manipulation and accelerated real-time PCR DNA amplification as well as quantification using a novel dual-modal Fe_3O_4 nanocluster.

reagents now contain Sybr Green dye. In contrast, iron oxide (Fe_3O_4) resists high temperatures because of its thermal stability. Yet the common nonstoichiometric structure of Fe_3O_4 makes it difficult to obtain photothermal properties in the near-infrared (NIR) wavelength region.[14,15] We therefore wanted to develop a photonic-PCR method with integrated magnetic-field-based molecular isolation and manipulation capabilities (Figure 1).

MATERIALS AND METHODS

Experimental procedures

Materials. Iron(II) chloride tetrahydrate ($FeCl_2{\bullet}4H_2O$, 99–102%) was purchased from Merck (Kenilworth, NJ, USA), trisodium citrate (100%) from JT Baker (Avantor Performance Materials Taiwan Co. Ltd., Chu-Bei City, Taiwan), benzene-1,3,5-tri-carboxylic acid (trimesic acid (TMA), 98%) and hydrazine monohydrate ($N_2H_4{\bullet}H_2O$, 67%) from Alfa Aesar (Thermo Fisher Scientific, Lancashire, UK)). Granular gelatin for analysis was purchased from ACROS (Echo Chemical Co. LTD, Toufen, Miaoli, Taiwan) and 1-ethyl-3-(3-dimethylaminopropyl) carbodiimide hydrochloride (EDC) from Sigma-Aldrich (St Louis, MO, USA).

Synthesizing the Fe_3O_4@Gelatin nanoclusters (NCs). The NIR-activated Fe_3O_4 NCs were prepared using a hydrothermal reaction for sub-gram-level preparations. In brief, $FeCl_2{\bullet}4H_2O$ (10 ml, 50 mM), TMA (4.5 ml, 25 mM), NaOH (18 mg), trisodium citrate ion (0.15 g), N_2H_4 (0.1 ml) and gelatin were mixed, stirred and then transferred to a 23-ml Teflon-lined stainless steel autoclave to be heated at 155 °C for 12 h. A repeated process of centrifugation and washing with deionized water was used to purify the as-synthesized Fe_3O_4 NCs.

Characterizing the particles. The shape and structure of the Fe_3O_4 NCs were analyzed using transmission electron microscopy at 80 kV (JEM-2000EXII; Jeol, Tokyo, Japan), high-resolution transmission electron microscopy at 300 kV (3010; Jeol) and field-emission scanning electron microscopy at 10 kV (XL-40 FEG; Philips, FEI Co., Hillsboro, OR, USA). NIR spectra were analyzed using an ultraviolet visible (UV-vis) spectrophotometer (8452A; Hewlett-Packard, Taipei, Taiwan). The magnetization curves (M–H) of Fe_3O_4 NCs were measured using a magnetometer (MPMS-7 SQUID; Quantum Design, San Diego, CA, USA) at 300 K. The powder pattern of nanoparticles was measured at BL01C2 at Taiwan's National Synchrotron Radiation Research Center (Hsinchu City, Taiwan). The wavelength of the incident X-rays was 1.03321 Å, and the diffraction patterns were recorded with a Mar345 imaging plate detector. The diffraction pattern was calibrated according to the Bragg positions of LaB6 standard with GSAS-II program. The NC cell parameters were refined using the Le Bail method and were quite similar to the standard inverse spinel structure of Fe_3O_4 NCs. The Fe_3O_4 NC solution was predissolved in 2 M HCl and the iron concentration of the Fe_3O_4 sample solution was quantified into p.p.m. unit by inductively coupled plasma atomic emission spectrometry (JY138 Spectroanalyzer; Horiba Jobin Yvon, Inc., Edison, NJ, USA).

Preparing Fe_3O_4@anti-D-Loop NCs. The as-prepared Fe_3O_4@Gelatin NCs were collected and washed three times with distilled water. To form Fe_3O_4@anti-D-Loop NCs, Fe_3O_4@Gelatin-*N*-hydroxysulfosuccinimide (NHS) conjugates were formed using EDC (18 mM) and NHS (18 mM). The amine-functionalized anti-D-Loop oligonucleotide (5′-TGG TAT TTT CGT CTG GGG GGT ATG-3′; 10 μl, 100 mM) was then added to the Fe_3O_4@Gelatin-NHS colloidal solutions (1 ml) at 4 °C and stirred for 24 h to produce Fe_3O_4@anti-D-Loop NCs for mitochondrial DNA (mtDNA) capture.

Cell culture. Healthy skin fibroblasts (1–3–16 cell line) and chronic progressive external ophthalmoplegia syndrome skin fibroblasts with 4977-bp-deleted cytoplasmic hybrids (cybrids) (51–12 cell line) were donated by Professor Y H Wei (Mackay Medical College, Institute of Biomedical Sciences, New Taipei City, Taiwan). In brief, the 1–3–16 cells were maintained in Dulbecco's Modified Eagle's Medium (DMEM) with 10% fetal bovine serum (FBS; Gibco, Invitrogen, Carlsbad, CA, USA) and 1% antibiotic–antimycotic agent (Gibco). The 51–12 cybrids were maintained in DMEM supplemented with 5% FBS, 100 μg ml^{-1} of pyruvate (Gibco) and 50 μg ml^{-1} of uridine (Sigma-Aldrich). All cells were maintained in a 37 °C incubator humidified with 5% CO_2 and 95% air.

MtDNA isolation protocol. An mtDNA extraction protocol (Mitochondria DNA Isolation Kit ab65321; Abcam, San Francisco, CA, USA) was used for the traditional PCR reaction. In brief, cells (10^6 cells ml^{-1}) were collected and washed with phosphate-buffered saline. The pellet was added to a 1× cytosol extraction buffer for 10 min of incubation on ice and then centrifuged at 1000 *g* for 10 min at 4 °C. Supernatant that contained mitochondria was then centrifuged at 12 000 *g* for 30 min at 4 °C. The mitochondria were then lysed using mitochondrial lysis buffer and incubated (Enzyme Mix; Abcam) (5 μl) for 60 min at 50 °C. The mtDNA samples were collected and centrifuged at

12 000 *g* for 5 min at room temperature, and the pellet was washed twice with 1 ml of 70% ethanol. After it had been air-dried for 5 min, the mtDNA was resuspended in 20 μl of water.

PCR setting for total mtDNA and 4977-bp deletion amplification. For traditional PCR, template DNA (100 ng) and Fe_3O_4 NCs (2500 p.p.m.$_{[Fe]}$) were added to a mixture containing 2× Mastermix (Sybr Fast qPCR Mastermix; Kapa Biosystems, Wilmington, MA, USA) and the primer pairs (5 μM of total mtDNA: L5604: 5′-cactctgcatcaactgaacg-3′, H5863: 5′-agtccaatgcttcactcagc-3′; and 4977-bp-deletion: L8395: 5′-caccataattacccccatactcctta-3′, H13494: 5′-gaggaaaggtattcctgctaatgc-3′) to a final standard reaction condition. Because of the same Tm value of the two primer pairs, multiplex PCR can be used. For photothermal PCR, ~500 cells μl^{-1} was used for template amplification. For traditional PCR, the cycle steps were programmed to amplify the template DNA using a thermal cycler (Veriti; Applied Biosystems, Foster City, CA, USA) as follows: the first stage at 95 °C for 10 min, the second stage (annealing at 58 °C for 30 s, extension at 72 °C for 30 s, denaturation at 95 °C for 30 s) for 40 amplification cycles, and a final stage at 72 °C for 10 min. For rapid photothermal PCR, the two cycle steps were programmed as follows: the first stage at 95 °C for 1 min and the second stage (annealing at 58 °C for 2 s, denaturation at 95 °C for 2 s) for 30–50 amplification cycles. The typical three-step PCR were programmed as follows: the first stage at 95 °C for 1 min, the second stage (annealing at 58 °C for 10 s, extension at 72 °C for 10 s, denaturation at 95 °C for 5 s) for 40 amplification cycles, and a final stage at 72 °C for 5 min.

RESULTS AND DISCUSSION

To synthesize the Fe_3O_4 NCs, a reduction environment was designed (with hydrazine [N_2H_4]) for reacting ferric chloride ($FeCl_2$), TMA, citrate ion and gelatin at 155 °C to produce high magnetization (117.3 emu per $g_{[Fe]}$) (Supplementary Figure S1) and the NIR absorption of Fe_3O_4 clusters. The resulting Fe_3O_4 NCs (Figure 2a) appear as a dense coating on a silicon (Si) wafer. A scanning electron microscopic micrograph shows uniform size of the Fe_3O_4 nanograins. The inset of Figure 2a shows a transmission electron microscopic image of a single Fe_3O_4 NC that consists of 10- to 11-nm cubic nanocrystals. Their hydrodynamic diameter was estimated to be about 110 nm, which suggested that the nanoparticle clusters had been formed in the solution system. In addition, the field-emission scanning electron microscopic image shows the individual Fe_3O_4 NCs that appeared in the diluted sample on calcium oxalate dehydrate crystals (Figure 2b). The Le Bail refinement method in high-resolution synchrotron X-ray powder diffraction pattern ($\lambda = 1.03321$ Å) of the Fe_3O_4 NCs was performed to determine the inverse spinel structure (Figure 2c). These peaks are matched with the standard Fe_3O_4 sample (28664-ICSD). The calculated 8.3873 Å of the unit cell constant identified very pure magnetite, because it is almost the same size as the standard Fe_3O_4 crystal ($a = 8.387$ Å). NIR spectrophotometric analysis showed a V-shaped optical absorption profile of the as-synthesized Fe_3O_4 NCs, with dual strong optical absorption windows appearing at 700 and ~1000 nm of the NIR biological optical window spectrum (Figure 2d). The inverse spinel-structured Fe_3O_4, with an intervalence charge transfer between Fe^{2+} and Fe^{3+}, allowed the Fe_3O_4 to have both high magnetization and intrinsic NIR absorbance.[16,17] The extinction at 808 and 1064 nm of Fe_3O_4 NCs remained around the initial intensity without significant depression over 7 days (Figure 3a), which suggested that the colloidal Fe_3O_4 NCs were stable. When irradiated with an NIR continuous wave (CW) laser diode (808 nm, 460 mW), the temperature of the Fe_3O_4 NCs (2500 p.p.m.$_{[Fe]}$) immediately rose to >100 °C and naturally cooled

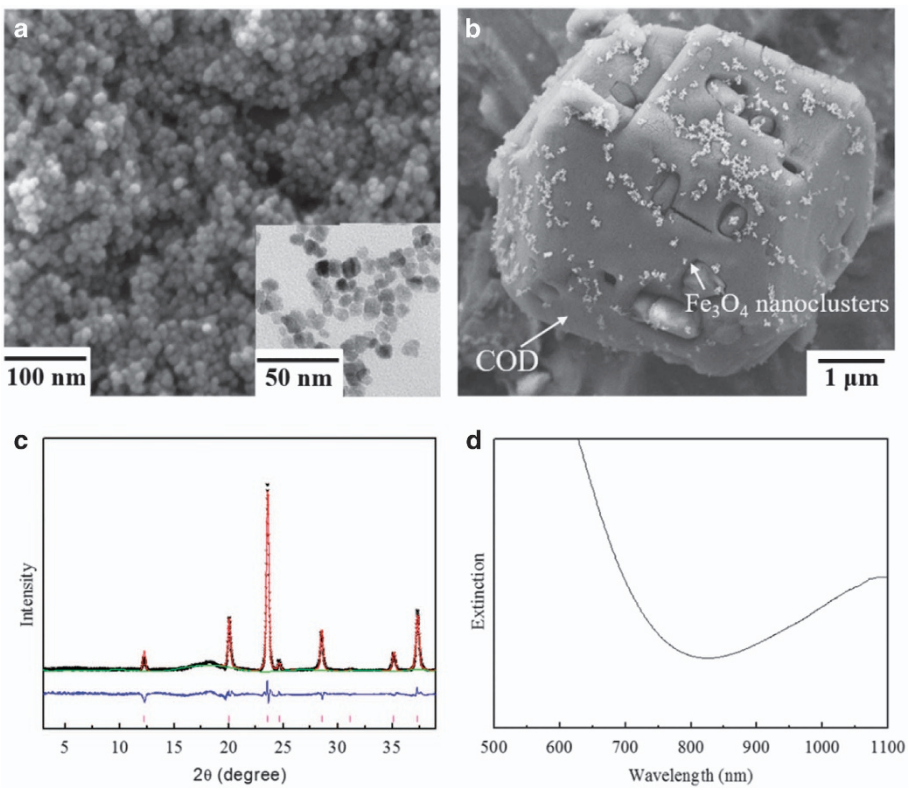

Figure 2 (**a**) Scanning electron microscope image of Fe_3O_4 nanoclusters. The inset shows a high-resolution transmission electron microscope micrograph of a single magnetite. (**b**) Near-infrared absorption of Fe_3O_4 nanoclusters using spectrometry. (**c**) XRD spectra in Fe_3O_4 nanoclusters using high-resolution synchrotron X-ray ($\lambda = 1.03321$ Å) source. (**d**) Near-infrared absorption of Fe_3O_4 nanoclusters using spectrometry.

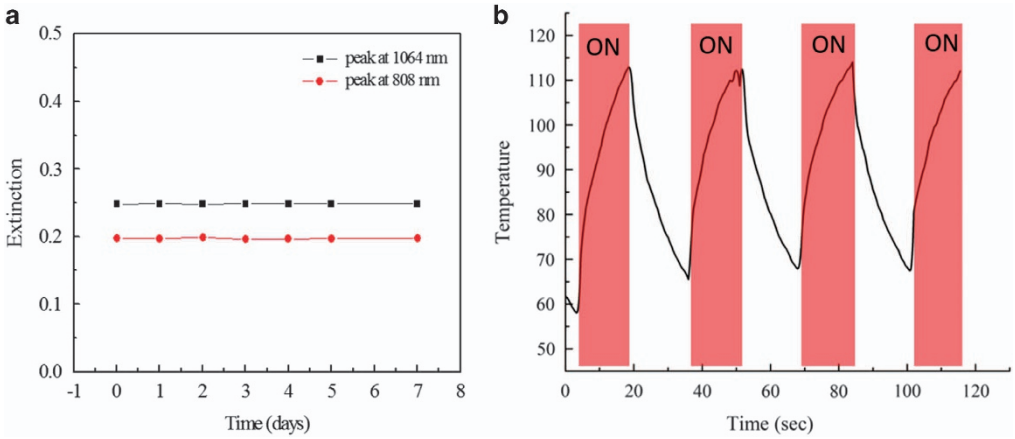

Figure 3 (**a**) The extinction at 808 and 1064 nm of Fe_3O_4 nanoclusters remained around the initial intensity without significant depression over 7 days. (**b**) Upon irradiation with laser diode peak at 808 nm (600 mW), the Fe_3O_4 nanoclusters (2500 p.p.m.) immediately heats up >100 °C and naturally cools down quickly when the irradiation is switched off.

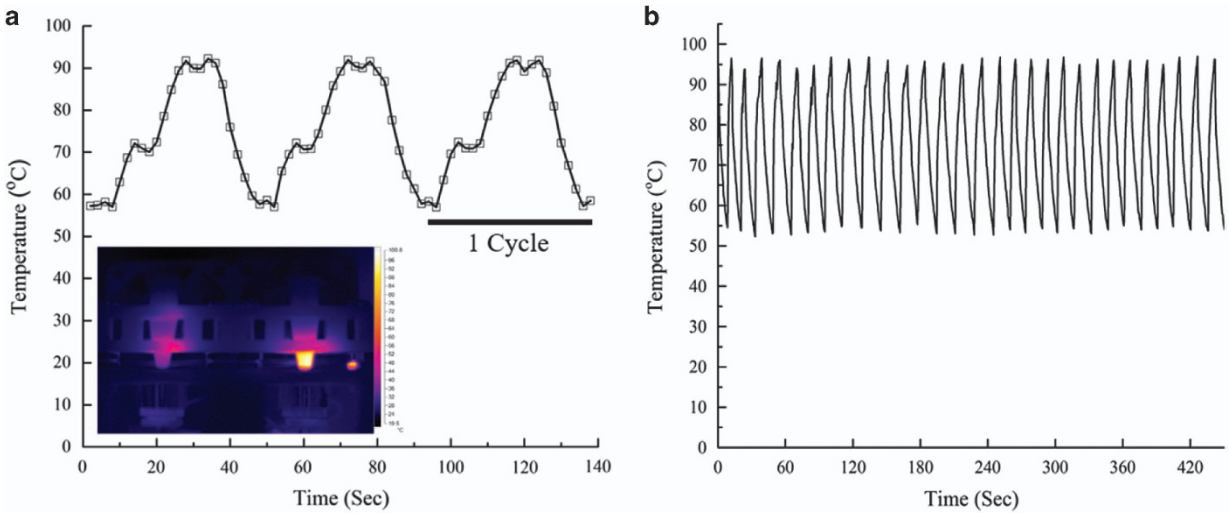

Figure 4 (**a**) The thermography record image (Ti32; Fluke Corp., Everett, WA, USA) showed that the temperature of a PCR tube containing 20 μl of an aqueous solution of a 2500-p.p.m. Fe_3O_4 nanocluster significantly rose to 90°C when it was irradiated with an NIR-CW laser diode (808 nm, 460 mW) for 15 s. (**b**) A K-type thermocouple was used to measure real-time dynamic temperature for the 30-thermal-cycle time requirement with 10 μl of an aqueous solution.

quickly when the radiation is turned off (Figure 3b). Particle stability was tested at room temperature for 3 months and no physical change was observed. Each batch was also tested for photothermal conversion efficiency and there were no significant differences between batches at the same NC concentration even after stored for 3 months (Supplementary Figure S2). These characteristics are sufficient for Fe_3O_4 NCs to act as the heating and cooling source for a nanothermal cycler.

We next evaluated whether Fe_3O_4 NCs significantly interfered with PCR-based DNA amplification. Fe_3O_4 NCs (2500 p.p.m.$_{[Fe]}$) were added to a mixture containing template DNA (100 ng), 2× master mix (Sybr Fast qPCR Mastermix; Kapa Biosystems) and two primer pairs (5 μM of total mtDNA: L5604: 5′-cactctgcatcaactgaacg-3′, H5863: 5′-agtccaatgcttcactcagc-3′; and 4977-bp deletion: L8395: 5′-caccataattacccccatactcctta-3′, H13494: 5′-gaggaaaggtattcctgctaat gc-3′) to a final standard reaction condition. A set of PCR cycle steps were programmed to amplify the template DNA using a thermal cycler (Veriti; Applied Biosystems) as follows: the first stage at 95 °C for 10 min, the second stage (annealing at 58 °C for 30 s, extension at 72 °C for 30 s, denaturation at 95 °C for 30 s) for 40 amplification cycles, and the final stage at 72 °C for 10 min. This showed that the nanoparticles did not compromise the efficiency of PCR amplification at the optimal annealing temperature (58 °C) (Supplementary Figure S3).

We then showed the potential of using Fe_3O_4 NCs in PCR with a photonic-modulated thermocycling device. The thermography record image (Ti32; Fluke Corp., Everett, WA, USA) showed that the temperature of a PCR tube containing 20 μl of an aqueous solution of a 2500 p.p.m.$_{[Fe]}$ Fe_3O_4 NC significantly rose to 90 °C when it was irradiated with an NIR-CW laser diode (808 nm, 460 mW) for 15 s (Figure 4a). It also revealed the homogenous distribution of the temperature in the reaction mixture with quantitative analysis illustrated (Supplementary Figure S4). The laser-pulse-modulated thermal cycle progression and the stability of the NCs during thermal cycling were tested using a K-type thermocouple placed in the solution for real-time dynamic temperature assessment. Using this NC, the

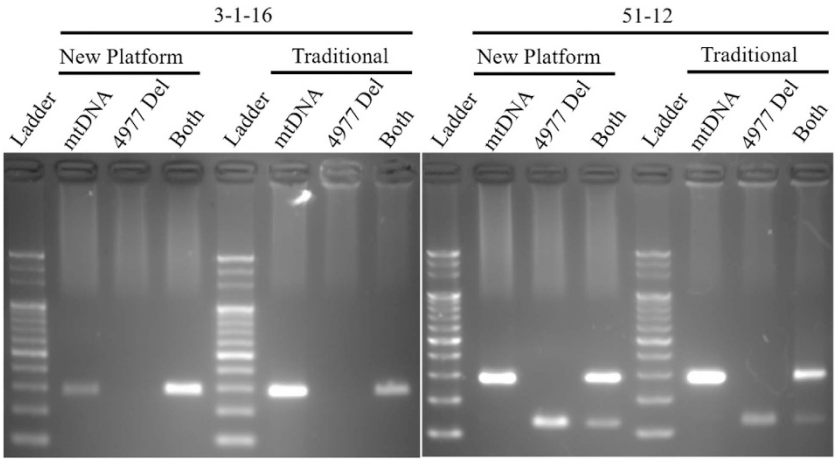

Figure 5 A comparison of traditional and photonic PCR using Fe_3O_4@anti-D-loop nanoclusters of mtDNA 4977-bps deletion detection in healthy skin fibroblasts (3-1-16) and a hybrid (51–12) with chronic progressive external ophthalmoplegia (CPEO) syndrome.

maximum attainable speed to complete 30 thermal cycles in a 10-μl reaction mixture was 420 s (Figure 4b).

In a mitochondrial disease model, this laser-pulse accelerated photonic-PCR system showed efficient quantitative clinical mutation detection. Alterations in mtDNA are well known to involve a wide variety of energy metabolism[18] and aging-associated diseases,[19] such as atherosclerosis, diabetes[20] and cancer.[21] Because mtDNA usually presents with heteroplasmy, a quantitative analysis to determine the proportion and types of mtDNA alterations is critical for diagnosing disease and for assessing how to treat it. Current mitochondrial disease detection requires tedious, time-consuming mtDNA extraction and subsequent quantitative analysis.[22] Thus an integrated method is highly desirable. Our quantitative photonic-PCR system combines, in a battery-powered portable device (Figure 1, bottom left photo), magnetic-particle-assisted DNA extraction, real-time quantitative DNA amplification and then determination of the mtDNA 4977-bps deletion.

The magnetic fields of the NCs were manipulated using magnetic nanoprobes with sequence-specific recognition of the mtDNA D-loop region. The probes had a surface conjugation of single-stranded DNA probes (5′-TGG TAT TTT CGT CTG GGG GGT ATG-3′) (anti-D-loop) using chemical crosslinks between gelatin on the nanoparticle surface and using EDC/NHS on the amine terminal group of DNA probes. Based on our calculations, the number of conjugated DNA probes per NC is approximately 119 strands (Supplementary Figure S5). We measured the mtDNA quantity captured by our NCs (~143 ng) and compared them with the quantity (~66 ng) obtained by a commercial kit (Abcam) using samples with an equal number of cells (10^6) (Supplementary Figure S6). These results showed that our magnetic isolation method was 217% more efficient than was the commercial kit.

The 51–12 cell line is a cybrid derived from the skin fibroblasts of a patient with chronic progressive external ophthalmoplegia syndrome.[23] This cell line presented typical 4977-bp mtDNA deletion at about 80% of total mtDNA. Cybrid line 1–3–16 from the same patient's healthy skin fibroblasts was the control. The mtDNA extraction was initiated using 500 cells premixed with Fe_3O_4@anti-D-loop NCs (20 μl) and then the solution temperature was raised to 95 °C using 5 min of laser irradiation. The NCs were then cooled to room temperature and the captured mtDNA was purified and concentrated with a magnet to remove the unbound suspension. Notably, the mtDNA capture agent does not contain inhibitors for neutralizing the cell lysate, which might develop an environment that can compromise the photonic-PCR process.

The photonic-PCR system consists of a microcontroller for DNA capture and PCR processing control. The critical temperature changes in PCR cycles were modulated by the pulse width of an NIR-CW laser diode (808 nm, 460 mW) that triggered the magnetic NC to generate precisely controlled heat feedback using a thermocouple placed in the PCR reaction mixture. A Bluetooth low-energy interface was designed for remote control and data transfer between a mobile device and the PCR system (Supplementary Figure S7). A two-step PCR protocol for 4977-bp deletion detection was completed within 600 s for 40 cycles using a conventional PCR tube with target abundance of the sample mtDNA down to 0.5 ng (Supplementary Figure S8). Although the PCR cycling time was efficient enough compared with conventional PCR, the speed could be further boosted up through controlling Fe_3O_4@anti-D-loop NC concentration (Supplementary Figure S9). Farrar and Witter[24] concluded that not only a greater concentration of critical reagent but also re-engineered DNA polymerase are both required to further accelerate PCR efficiency. In addition, the typical three-step photonic-PCR system also derived an amplified DNA product with similar fluorescent intensity on Sybr Green-stained electrophoresis gel (Figure 5). Moreover, the photonic system is much more time efficient (35 versus 100 min) than is traditional PCR. It is worth pointing out that the system was evaluated using a multiplex PCR design that has not been reported before in previous portable ultra-efficient PCR systems. We hypothesize that such improved DNA enrichment is attributable to accelerated mixing by the magnetic 'hot particle' (Fe_3O_4@anti-D-loop) to promote the interaction of template DNA with primers while simultaneously serving as the endogenous heat source, which accelerates overall PCR cycle progression.

Finally, we demonstrated real-time qPCR detection by integrating the portable photonic PCR device with a 450-nm blue laser diode (Egismos Technology Corp., Burnaby, BC, Canada) and an ultra-high sensitive CMOS camera detector. This optic setup provides high signal-to-noise ratio. The optical intensity signal from Sybr Green fluorescence (excitation: 488 nm; emission: 520 nm) that corresponds to the total amount of double-stranded DNA was detected on all 50 cycles and analyzed using the Omnivision OVTAPantherM software (Figure 6). The results indicated that the Fe_3O_4 NCs did not interfere with the Sybr Green fluorescence signal detection at the reaction

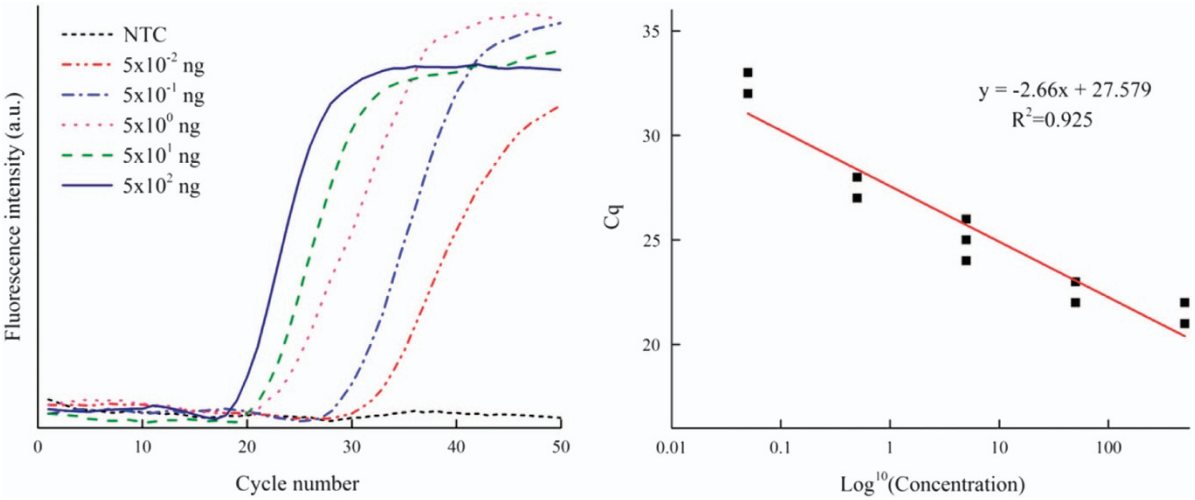

Figure 6 Demonstration of real-time quantitative PCR detection by integrating the portable photonic PCR device using a 450-nm blue laser diode (Egismos Technology Corp., Burnaby, BC, Canada) and a CMOS detector. The optical signal intensities from the Sybr Green fluorescence were analyzed using the Omnivision OVTAPantherM software.

concentration. We showed stable detection of mtDNA 4977-bp deletion. At least four serial dilutions of the initial template (50 pg ~ 500 ng) were detectable and the Cq values can be calculated with reasonable linearity.

CONCLUSIONS

This is the first report of the successful integration of a highly efficient magnetic field molecular manipulation and accelerated real-time PCR DNA amplification and quantification using a novel dual-modal Fe_3O_4 NC that provides photothermal conversion and has magnetic properties. No other PCR study has used Fe_3O_4 NCs as the NIR-modulated heat generator or reported accelerated DNA amplification with the same reaction volume and thermal cycles. This is also the first report to show multiple PCR in a one-tube reaction without separate preextraction. The system has also been successfully used to detect *Clostridium difficile* infection (Supplementary Figure S10) and the ankylosing spondylitis risk gene (data not shown), which has a final amplicon size of <1 kb. We believe the advantage of this development is a milestone toward an advanced ultraportable PCR and qPCR system. This would establish the bases for next-generation chip-PCR/microarray and *in situ* optical PCR. The nano-heating/-cooling module can now be realized by the interaction of magnetic nanoparticles and electromagnetic wave at low volume. Temperature changes in any area of the field were controlled using optical modulation (Supplementary Figure S11). Our developed energy-efficient portable magneto-optical real-time qPCR device will enable a novel class of Fe_3O_4 nanoparticles to pave the way toward using advanced PCR technologies in point-of-care devices.

CONFLICT OF INTEREST

The authors declare no conflict of interest.

ACKNOWLEDGEMENTS

We thank the National Cheng Kung University and Molecular Medicine Core Laboratory, Research Center of Clinical Medicine, National Cheng Kung Hospital for providing technical support and assistance with experimental design. We thank the National Science Council in Taiwan for financial support provided to this study by grant MOST 104-2627-M-006-001.

1 Mullis, K., Faloona, F., Scharf, S., Saiki, R., Horn, G. & Erlich, H. Specific enzymatic amplification of DNA in vitro: the polymerase chain reaction. *Cold Spring Harb. Symp. Quant. Biol.* **51**, 263–273 (1986).
2 Oda, R. P., Strausbauch, M. A., Huhmer, A. F., Borson, N., Jurrens, S. R., Craighead, J., Wettstein, P. J., Eckloff, B., Kline, B. & Landers, J. P. Infrared-mediated thermocycling for ultrafast polymerase chain reaction amplification of DNA. *Anal. Chem.* **70**, 4361–4368 (1998).
3 Fermer, C., Nilsson, P. & Larhed, M. Microwave-assisted high-speed PCR. *Eur. J. Pharm. Sci.* **18**, 129–132 (2003).
4 Zhu, Z., Jenkins, G., Zhang, W. H., Zhang, M. X., Guan, Z. C. & Yang, C. J. Single-molecule emulsion PCR in microfluidic droplets. *Anal. Bioanal. Chem.* **403**, 2127–2143 (2012).
5 Belaud-Rotureau, M. A., Parrens, M., Dubus, P., Garroste, J. C., de Mascarel, A. & Merlio, J. P. A comparative analysis of FISH, RT-PCR, PCR, and immunohistochemistry for the diagnosis of mantle cell lymphomas. *Mod. Pathol.* **15**, 517–525 (2002).
6 Watkins-Riedel, T., Woegerbauer, M., Hollemann, D. & Hufnagl, P. Rapid diagnosis of enterovirus infections by real-time PCR on the LightCycler using the TaqMan format. *Diagn. Microbiol. Infect. Dis.* **42**, 99–105 (2002).
7 Zhou, C., Liu, D., Xu, L., Li, Q., Song, J., Xu, S. H., Xing, R & Song, H. A sensitive label-free amperometric immunosensor for alpha-fetoprotein based on gold nanorods with different aspect ratio. *Sci. Rep.* **5**, 9939 (2015).
8 Hu, K. W., Huang, C. C., Hwu, J. R., Su, W. C., Shieh, D. B. & Yeh, C. S. A new photothermal therapeutic agent: core-free nanostructured Au_xAg_{1-x} dendrites. *Chem. Eur. J.* **14**, 2956–2964 (2008).
9 Kennedy, L. C., Bickford, L. R., Lewinski, N. A., Coughlin, A. J., Hu, Y., Day, E. S., West, J. L. & Drezek, R. A. A new era for cancer treatment: gold-nanoparticle-mediated thermal therapies. *Small* **7**, 169–183 (2011).
10 Li, H., Huang, J., Lv, J., An, H., Zhang, X., Zhang, Z., Fan, C. & Hu, J. Nanoparticle PCR: nanogold-assisted PCR with enhanced specificity. *Angew. Chem. Int. Ed.* **44**, 5100–5103 (2005).
11 Li, M., Lohmüller, T. & Feldmann, J. Optical injection of gold nanoparticles into living cells. *Nano Lett.* **15**, 770–775 (2015).
12 Chen, C. C., Lin, Y. P., Wang, C. W., Tzeng, H. C., Wu, C. H., Chen, Y. C., Chen, C. P., Chen, L. C. & Wu, Y. C. DNA-gold nanorod conjugates for remote control of localized gene expression by near infrared irradiation. *J. Am. Chem. Soc.* **22**, 3709–3715 (2006).
13 Son, J. H., Cho, B., Hong, S., Lee, S. H., Hoxha, O., Haack, A. J. & Lee, L. P. Ultrafast photonic PCR. *Light Sci. Appl.* **4**, e280 (2015).
14 Chen, H., Burnett, J., Zhang, F., Zhang, J., Paholak, H. & Sun, D. Highly crystallized iron oxide nanoparticles as effective and biodegradable mediators for photothermal cancer therapy. *J. Mater. Chem. B* **2**, 757–765 (2014).
15 Huang, C. C., Chang, P. Y., Liu, C. L., Xu, J. P., Wu, S. P. & Kuo, W. C. New insight on optical and magnetic Fe_3O_4 nanoclusters promising for near infrared theranostic applications. *Nanoscale* **7**, 12689–12697 (2015).
16 Tang, J., Myers, M., Bosnick, K. A. & Brus, L. E. Magnetite Fe_3O_4 nanocrystals: spectroscopic observation of aqueous oxidation kinetics. *J. Phys. Chem. B* **107**, 7501–7506 (2003).
17 Liao, M. Y., Wu, C. H., Lai, P. S., Yu, J., Lin, H. P., Liu, T. M. & Huang, C.-C. Surface state mediated NIR two-photon fluorescence of iron oxides for nonlinear optical microscopy. *Adv. Funct. Mater.* **23**, 2044–2051 (2013).
18 Fernie, A. R., Carrari, F. & Sweetlove, L. J. Respiratory metabolism: glycolysis, the TCA cycle and mitochondrial electron transport. *Curr. Opin. Plant Biol.* **7**, 254–261 (2004).
19 Bratic, A. & Larsson, N. G. The role of mitochondria in aging. *J. Clin. Invest.* **123**, 951–957 (2013).

20 Lane, R. K., Hilsabeck, T. & Rea, S. L. The role of mitochondrial dysfunction in age-related diseases. *Biochim. Biophys. Acta.* **1847**, 1387–1400 (2015).
21 Wallace, D. C. Mitochondria and cancer. *Nat. Rev. Cancer* **12**, 685–698 (2012).
22 Lang, B. F. & Burger, G. Purification of mitochondrial and plastid DNA. *Nat. Protoc.* **2**, 652–660 (2007).
23 Liu, C. Y., Lee, C. F. & Wei, Y. H. Quantitative effect of 4977 bp deletion of mitochondrial DNA on the susceptibility of human cells to UV-induced apoptosis. *Mitochondrion* **7**, 89–95 (2007).
24 Farrar, J. S. & Wittwer, C. T. Extreme PCR: efficient and specific DNA amplification in 15-60seconds. *Clin. Chem.* **61**, 145–153 (2015).

Supplementary Information accompanies the paper on the NPG Asia Materials website (http://www.nature.com/am)